Published online 12 January 2012 *Nucleic Acids Research, 2012, Vol. 40, No. 9* ***4203–4215***
doi:10.1093/nar/gkr1286

G-quadruplex structure and stability illuminated by 2-aminopurine phasor plots

Robert Buscaglia[1], David M. Jameson[2] and Jonathan B. Chaires[1,*]

[1]James Graham Brown Cancer Center, University of Louisville, 505 S. Hancock Street, Louisville, KY 40202 and [2]Department of Cell and Molecular Biology, John A. Burns School of Medicine, University of Hawaii, Honolulu, HI 96813, USA

Received October 27, 2011; Revised December 13, 2011; Accepted December 15, 2011

ABSTRACT

The use of time-resolved fluorescence measurements in studies of telomeric G-quadruplex folding and stability has been hampered by the complexity of fluorescence lifetime distributions in solution. The application of phasor diagrams to the analysis of time-resolved fluorescence measurements, collected from either frequency-domain or time-domain instrumentation, allows for rapid characterization of complex lifetime distributions. Phasor diagrams are model-free graphical representations of transformed time-resolved fluorescence results. Simplification of complex fluorescent decays by phasor diagrams is demonstrated here using a 2-aminopurine substituted telomeric G-quadruplex sequence. The application of phasor diagrams to complex systems is discussed with comparisons to traditional non-linear regression model fitting. Phasor diagrams allow for the folding and stability of the telomeric G-quadruplex to be monitored in the presence of either sodium or potassium. Fluorescence lifetime measurements revealed multiple transitions upon folding of the telomeric G-quadruplex through the addition of potassium. Enzymatic digestion of the telomeric G-quadruplex structure, fluorescence quenching and Förster resonance energy transfer were also monitored through phasor diagrams. This work demonstrates the sensitivity of time-resolved methods for monitoring changes to the telomeric G-quadruplex and outlines the phasor diagram approach for analysis of complex time-resolved results that can be extended to other G-quadruplex and nucleic acid systems.

INTRODUCTION

Fluorescence techniques offer valuable tools for investigating the structure, polymorphism and interactions of nucleic acid systems. The fluorescent adenine analog 2-aminopurine (2AP) has been widely used in the study of nucleic acid systems because of its favorable fluorescent properties, particularly its high quantum yield and its excitation wavelength that is significantly red-shifted from the absorbance region of protein and the natural occurring bases (1). Because of its advantageous fluorescence properties, 2AP allows for the investigation of protein/DNA systems including DNA and RNA polymerases (2,3), and has been widely used to characterize RNA and DNA structure and dynamics (4–8).

Although the steady-state fluorescence of 2AP is relatively simple and can provide information on the nucleic acid system through emission intensity changes, time-resolved measurements have the potential to provide more insight into underlying photophysical processes. The lifetime of 2AP free in aqueous solution is a single exponential decay with a lifetime of ~10–11 ns (9,10). Upon incorporation into a nucleic acid polymer or oligonucleotide, the decay of 2AP fluorescence becomes complex with multiple lifetimes ranging from 8 ns to 50 ps (9). Recent investigations have attempted to describe the fluorescent lifetime of 2AP within a nucleic acid polymer as a distribution of lifetimes rather than discrete lifetime states (10,11). The photophysical changes of 2AP upon incorporation into nucleic acid polymers have been extensively studied. Titration of 2AP with nucleosides or nucleoside triphosphates established the importance of base stacking in the quenching of 2AP fluorescence and the emergence of multiple lifetimes (12). Computational approaches evaluating the electronic structure of 2AP through time-dependent density functional theory confirmed the static and dynamic quenching of the 2AP fluorescence arising from base stacking. Other computational studies also revealed multiple electronic states upon excitation that were proposed to result in shortened excited state lifetimes and the formation of new non-radiative transitions (13,14).

*To whom correspondence should be addressed. Tel: +1 502 852 1172; Fax: +1 502 852 1153; Email: j.chaires@louisville.edu

Interpretation of time-resolved fluorescence data typically requires model fitting to determine lifetimes and fractional intensities [with the exception of the Maximum Entropy Method (15)]. Non-linear regression analysis for lifetime determination depends on the model chosen to best represent the data. Model fitting can become increasingly complicated when solutions contain multiple lifetimes. Samples containing multiple lifetimes, arising either from a mixture of fluorophores or fluorophores with complex lifetime distributions, require increased time for analysis and present difficulty in resolving unique models. This complexity has limited the use of time-resolved methods in nucleic acid studies.

Simplification of time-resolved data analysis may be accomplished through the use of phasor diagrams, which are model-free graphical representations of transformed time-resolved fluorescence results (16). Phasor plots have antecedents in Cole–Cole plots (17), and appear under a variety of names in fluorescence studies, such as AB-plots (18) and polar plots (19). Equations 1 and 2 give the (x,y) transformation of frequency-domain lifetime measurements into a 2D (G,S) phasor plot for graphical representation of time-dependent results.

$$x = G = M\cos\phi \quad (1)$$

$$y = S = M\sin\phi \quad (2)$$

Measurement of the modulation ratio (M) and phase delay (ϕ) are directly acquired from frequency-domain instrumentation, but there exists direct transformations to the (G,S) space for time-domain measurements (16,19–21). This simplified analysis removes both the non-linear regression and model-dependent assumptions, facilitating an immediate analysis of time-dependent results. At a fixed modulation frequency, fluorophores that exhibit a single exponential decay will result in a phasor point that falls on the so-called universal circle, described by a semicircle with radius one-half centered at $(0.5, 0)$. The position of the lifetime along the universal circle is dependent on the modulation frequency used for the time-dependent measurement. An immediate conclusion can be drawn that a single lifetime is present in solution if the phasor point lies on the universal circle. If the solution contains a mixture of fluorophores with unique single-exponential lifetimes or a single fluorophore that exhibits multiple exponential decays, the phasor point will fall within the universal circle. Although the phasor analysis will be unable to directly determine the exact distribution of lifetimes in solution without further analysis, any phasor points that fall within the universal circle are known to contain a mixture of fluorescent decays. Excited state reactions cause movement of the phasor points outside the universal circle. Examples include FRET monitored by lifetime changes of the acceptor fluorophore and solvent relaxation (16,22).

The placement of the phasor point of a complex mixture can be described as the linear combination of single exponential phasor points (Figure 1). As stated earlier, two fluorophores having single exponential lifetimes will exhibit phasor points that fall along the universal circle. A mixture of the single-exponential fluorophores will result in a phasor point that lies at a position within the universal circle along the line segment connecting the two single exponential phasor points (16). Importantly, any movement in the position of the phasor point indicates changes in the lifetimes or fractional intensities. Sensitive time-dependent measurements are simplified to movements of the phasor point that establish interactions and dynamics of the system. Phasors allow for rapid interpretation of time-dependent lifetime results and can be used to determine changes in the local environment of the fluorophore being monitored, resulting in simplified analysis of fluorophore mixtures, structural changes and binding interactions.

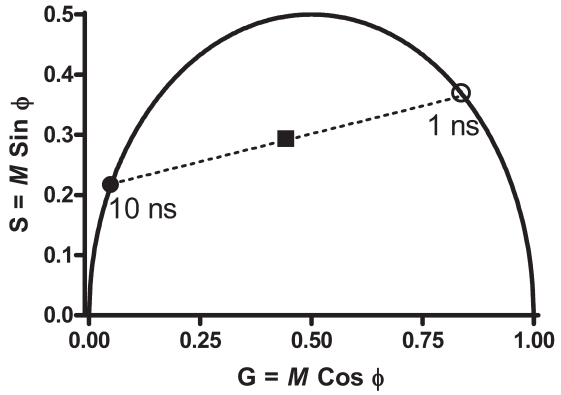

Figure 1. Construction of a phasor point for a mixture of two single-exponential lifetimes in solution. Phase and modulation data were simulated using a frequency of 70 MHz. The phasor points corresponding to single exponential decays of 10 ns (closed circle) and 1 ns (open circle) fall on the universal circle. A mixture of these two fluorophores in solution would result in two exponential decays, resulting in a phasor point falling within the universal circle. The phasor point would fall along the line segment connecting the two unique single exponential decays, with the position of the point dependent on the fractional intensity composition of the mixture. The phasor point shown (closed box) represents 1:1 fractional intensities of 10 and 1 ns species in solution, resulting in a phasor point that lies directly between the two points on the universal circle.

Phasor diagrams have become an important tool for time-dependent fluorescence microscopy studies due to improved data analysis routines and simplification of lifetime results and FRET efficiency calculations (19,23–25). Recently, *in vitro* studies of protein systems and their analysis by phasor diagrams were presented, simplifying complex analysis of time-dependent data and making interpretation of often complex results accessible to non-experts (16,26). Phasor analysis has been used to enhance fluorescence microscopy and *in vitro* protein studies, whereas extension of the method into nucleic acid studies has yet to be described. The effectiveness of phasors for analysis of complex nucleic acid systems is described here through the use of the 22-nt 5′-d(AGGG $(TTAGGG)_3$) human telomeric G-quadruplex forming oligodeoxynucleotide (ODN).

G-quadruplexes are structures containing two or more stacked square-planar G-tetrads composed of four Hoogstein hydrogen bonded guanines. G-quadruplexes may form from the tetramolecular association of four strands, the bimolecular association of two strands, or

from the unimolecular folding of one strand. In the later two cases, strand segments align in parallel or anti-parallel arrangements joined by a variety of single-strand loops (27). G-quadruplex structures are stabilized by the coordination of a cation, typically sodium or potassium, with the O6 of the guanine residues within the cavity of the G-tetrads (28). The human telomeric G-quadruplex sequence folds into a variety of conformations depending on solution composition and sequence modifications (29). These diverse conformations feature unique strand segment orientations and loop types. G-quadruplex structures adopt conformations containing parallel, anti-parallel or (3 + 1) mixed strand segment orientations. Loop types include diagonal, edgewise and double-chain reversal. Each of these strand orientations and loop types are found in telomeric G-quadruplex DNA structures; an all parallel double chain reversal structure (30), two anti-parallel structures containing one diagonal and two edgewise loops (31–33), as well as two (3 + 1) mixed structures containing two edgewise and a double-chain reversal loop (34–38). Telomeric G-quadruplex formation in the presence of potassium favors 'hybrid' structures with two edgewise loops and one double-chain reversal loop, whereas only a single predominant anti-parallel 'basket' structure has been found in the presence of sodium (29).

Because the core quartet stacks of telomeric G-quadruplex structures are similar, studies that focus on strand orientation and loop-type can potentially differentiate telomeric G-quadruplex structures. Techniques sensitive to changes in local environment, particularly fluorescence, are especially important for this purpose. Although steady-state fluorescence techniques have been widely used to investigate G-quadruplex structures, only a relatively few time-resolved fluorescence investigations have been reported (39,40). Incorporation of 2AP into the loops of the telomeric G-quadruplex sequence has aided thermodynamic and kinetic studies of G-quadruplex folding, providing a signal that is sensitive to a local structural environment that complements the measurement of global folding or other structural transitions (41–43). Solution FRET and single-molecule FRET studies have elucidated conformational heterogeneity of the telomeric structures (44,45). The use of FRET pairs plays an important role in high-throughput thermal melting assays to explore the stability of G-quadruplex structures and potential ligands (46,47).

This study evaluates 2AP-incorporated or FRET-labeled telomeric G-quadruplex forming ODNs through the use of time-resolved instrumentation and phasor diagram analysis. Our results show that such time-resolved methods reveal subtleties in a number of G-quadruplex structural transitions that are not evident in steady-state measurements, aiding the elucidation of the underlying reaction mechanisms.

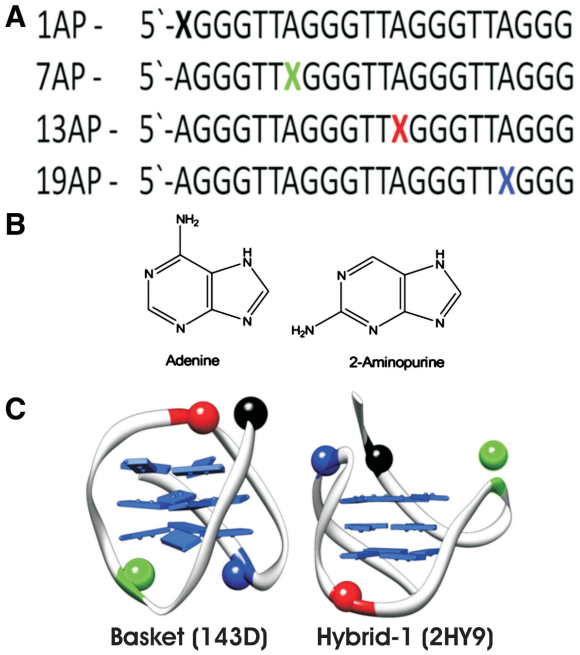

Diagram 1. (**A**) 2AP substituted G-quadruplex forming sequences derived from the human telomeric repeat. The diagram gives the abbreviations used for the different 2AP-substituted 22-nt deoxyoligonucleotide sequences along with a color-coded format used for all phasor plots. The bold X in each sequence corresponds to the placement of the 2AP in the 22-base sequence. (**B**) A comparison of the chemical structures of adenine and its fluorescent analog 2AP. (**C**) A comparison of two published human telomeric G-quadruplex conformations (143D and 2HY9) highlighting where the 2AP-substitutions (colored spheres) would be located within these distinct G-quadruplex conformations. Blue planar rectangles represent guanine residues in the formation of G-tetrad cores. The sequentially labeled telomeric forming G-quadruplex sequences will cause the fluorescent 2AP probe to localize differently dependent on the conformation and can be used to locally probe the loop environment.

MATERIALS AND METHODS

Oligodeoxynucleotides and sample preparation

Unlabeled and 2AP-labeled 5′-d(AGGG(TTAGGG)$_3$) were purchased from Integrated DNA Technologies (Coralville, IA, USA). All ODNs were purchased on a 5-μmol scale with standard desalting. Four unique 2AP-labeled ODNs were purchased with substitutions at positions 1, 7, 13 and 19 corresponding to a single adenine change to 2AP (Diagram 1). Fluorescently tagged 6FAM-d(AGGG(TTAGGG)$_3$)-TAMRA ODNs were purchased from Sigma (St Louis, MO, USA) on a 10-μmol scale with standard desalting and HPLC purification. ODNs are quality checked by commercial sources through the use of either MALDI-TOF or Electrospray Ionization mass spectrometry. All purchased ODNs were used without further purification. Fluorescent tag abbreviations are 6-carboxyfluorescein (6FAM) and tetramethylrhodamine (TAMRA). Prior to use, DNAs were diluted into folding buffer (10 mM tetrabutylammonium phosphate, 1 mM EDTA acid, pH 7.1) to a stock concentration of 1 mM and stored at 4°C. Folding buffer represents a potassium and sodium-free solvent resulting in minimal G-quadruplex formation prior to the addition of added cation. Folding buffer solutions are used to provide a defined initial state so the effects of added cation can be clearly identified. Unless otherwise stated, all experimental samples were annealed prior to use by

placement in boiling water for 10 min followed by quenching on ice for 10 min. All fluorescent standards and reagents were purchased at the highest available grade from Sigma. Fluorescent standards were prepared at stock concentrations of 1 mg/ml and diluted to experimental concentrations for matched intensities with samples using the following solvents: *p*-terphenyl (τ = 1.05 ns) in ethanol, fluorescein (τ = 4.1 ns) in 0.1 M NaOH and 2AP (τ = 10.5 ns) in folding buffer. Stock solutions of 1 M NaCl, 1 M KCl and 3 M acrylamide were prepared in folding buffer.

A concern whenever an oligonucleotide is modified by a base substitution is that the native structure might be perturbed. For 2AP substitutions, circular dichroism and thermal denaturation measurements were used to show that the global G-quadruplex structure was minimally perturbed in modified sequences, as was observed and reported earlier (43). In addition, steady-state fluorescence properties of 2AP substituted at specific loop sites were found to correlate with solvent accessible surface areas of adenine residues in atomic-resolution models of G-quadruplex structures (42), suggesting that the modified base accurately reports on the local loop environment.

Steady-state and time-resolved fluorescence spectroscopy

All steady-state scans were collected on a Horiba Scientific (Edison, NJ, USA) Fluoromax 3 equipped with a circulating water bath. Time-resolved data were acquired on an ISS (Champaign, IL, USA) K2 multi-frequency cross-correlation phase and modulation fluorometer equipped with a circulating water bath and either a 300-nm LED for 2AP-labeled samples or a 472-nm LED for 6FAM labeled samples. All time-resolved scans were completed with polarizers set to magic angle conditions and with emission path length cutoff filters passing wavelengths >380 nm for the 300-nm LED and 515 nm for the 472-nm LED to negate the collection of stray light (48). Sample and references were scanned using 1 cm path length Starna (Atascadero, CA, USA) quartz microvolume cuvettes with an optimal volume of 800 µl. Samples were maintained at a constant temperature of 20°C. Non-linear regression analysis of fluorescence lifetime data was conducted using Globals software (49).

Phasor preparation

For each set of phase delay (ϕ) and modulation ratio (M) values collected, a phasor point was constructed using an Excel spreadsheet to calculate the values of G and S (Equations 1 and 2) at the reported modulation frequency. Deviations of S and G were calculated using Equations 3 and 4.

$$\delta_G = \sqrt{(S \times \delta_\phi)^2 + (\cos\phi \times \delta_M)^2} \quad (3)$$

$$\delta_S = \sqrt{(G \times \delta_\phi)^2 + (\sin\phi \times \delta_M)^2} \quad (4)$$

Equations 3 and 4 represent the SD of the G (δ_G) and S (δ_S) components where $\delta\phi$, the SD of the phase delay, and δ_M, the SD of the modulation ratio, are recorded from time-resolved measurements. Evaluation of the errors associated with S and G can be used to establish significant movements of the phasor point. A universal circle was constructed using Mathematica 9.0 to generate 1000 points of a semicircle centered at (0.5, 0) with a radius of 0.5. All phasor diagrams were plotted using Prism GraphPad software.

Cation titrations

2AP-labeled ODNs or dual-labeled FRET ODNs were diluted from stock to an approximate strand concentration of 2 µM using folding buffer. Background checks of folding buffer alone and cation into folding buffer gave total intensity counts of <1% of the sample signals, resulting in negligible contributions from background to the total observed intensity. Cation titrations were completed by the addition of aliquots of either 100 mM or 1 M NaCl or KCl into the sample cuvette followed by thorough mixing and 5-min equilibration periods. Single frequency phase and modulation scans were collected by setting a fixed modulation frequency (93 MHz) and iterating scans over 360 s with a time step of 30 s, resulting in the acquisition of 13 scans per sample point. Instrumental scan parameter ESE% was set to 0.18 to reduce collected phase and modulation value deviations using an iteration maximum of 250. Cation concentration ranged from 0 to 100 mM over 28 points.

Mung bean nuclease digestions

Digestion of 2AP-labeled ODNs by the single-strand specific mung bean nuclease was monitored using single frequency phase and modulation data acquisition (93 MHz). Samples were prepared by dilution of 2AP-labeled ODNs from stock to 2 µM strand concentration using a digestion buffer (50 mM potassium acetate, 100 mM potassium chloride, 1 mM zinc sulfate, pH 5.0). Single frequency scans were acquired in the absence of mung bean nuclease to establish an initial phasor point. Digestion of the labeled ODNs was monitored over 26 010 s with data acquisition every 45 s after the addition and thorough mixing of mung bean nuclease to 1 U/µl. Digestions were similarly completed and monitored using steady-state fluorescence emission intensities. Samples were prepared in digestion buffer at strand concentrations of 2 µM. Data collection was conducted by excitation of the sample at 305 nm with emission monitored at 370 nm with excitation and emission slit widths of 5 nm and 1 s integration times. Data acquisition was trigged after thorough mixing of mung bean nuclease into the sample at 1 U/µl and monitored over 20 000 s with data collection every 5 s. Digestions were completed at 20°C.

Acrylamide quenching

Steady-state fluorescence emission intensity and time-resolved lifetimes of 2AP were monitored after

the addition of the fluorescence quencher acrylamide. Separate samples for each acrylamide concentration were prepared by dilution of stock ODNs to 2 μM strand concentration. Samples contained 25 mM KCl or 50 mM NaCl and acrylamide ranging from 0 to 0.55 M. The samples were diluted to a final volume of 2 ml by folding buffer. After sample preparation, ODNs were allowed to equilibrate overnight at room temperature in the dark. Data collection was then acquired on all samples using both steady-state fluorescence emission scans and multiple-frequency phase and modulation scans. Steady-state emission scans were collected with excitation at 305 nm and emission scanned from 320 to 440 nm every 1 nm, with 1 s integration and 5-nm excitation and emission slit widths. Lifetime scans were acquired using multi-frequency phase and modulation scans from 10 to 150 MHz over 10 points on a log base 2 scale. ESE% was set to 0.18 with a maximum of 250 iterations. The average of four scans is reported for all samples. This sample preparation and data acquisition protocol allowed identical samples to be scanned in both steady-state and time-resolved fluorometers for direct comparison of quenching profiles using fluorescence emission intensity and lifetimes. Phasor diagrams were prepared using the 49-MHz phase and modulation scans for all acrylamide concentrations.

RESULTS AND DISCUSSION

Time-resolved evaluation of 2AP-substituted telomeric G-quadruplex DNA

The four ODNs shown in Diagram 1 were used to probe loop regions of the G-quadruplex structure formed by the human telomere 22 base sequence 5′-d(AGGG(TTA GGG)$_3$). The structure of 2AP is shown to highlight the chemical change to the purine necessary for increased quantum yield and improved fluorescence studies. The 2AP differs from adenine by relocation of the amine group from position 6 to position 2. Diagram 1 highlights two unique human telomeric G-quadruplex conformations and their distinctive 2AP environments. The four chosen substitutions place a 2AP residue in successive loops, beginning with a single 5′-flanking residue and stepping through each of the three loops formed by the monomolecular telomeric G-quadruplex. These strategic substitutions confer the ability to explore the localized environment of the 2AP residue within the G-quadruplex loop, and can be used to draw conclusions about the loop environment. The same 2AP substitutions have been previously reported from steady-state investigations and were used to draw conclusions about possible G-quadruplex conformations present in solution (43). The resulting steady-state fluorescence emission curves for the four 2AP-substiuted ODNs were measured under the experimental conditions used for this study (Supplementary Figure S1). The normalized fluorescence emission intensities show the ability of 2AP to probe the local loop environments. Differences in 2AP fluorescence at specific positions are seen in the presence of sodium or potassium. Such differential 2AP fluorescence quenching indicates different loop environments, probably due to differences in base stacking (12–14). Although measurement of emission intensities provide information about the local environment of G-quadruplex loops, steady-state methods are of limited resolution and may not reveal local or global conformational heterogeneity (29).

Time-resolved measurements offer the opportunity to evaluate more subtle differences in loop environments, with potential for revealing conformational heterogeneity. Figure 2 illustrates the complication of measuring the lifetime of 2AP upon incorporation into a nucleic acid polymer. Measurement of a 2AP residue free in solution (Figure 2A) results in a single exponential decay with a lifetime of 10.4 ns, in agreement with published results (9,10). Upon substitution into G-quadruplex structures, however, the data (Figure 2B) cannot be fitted by a single lifetime, and more complex models are required. Supplementary Table S1 reports both the lifetimes and fractional intensities resulting from non-linear regression analysis of all four individual 2AP-substituted ODNs in the presence of 25 mM KCl. Several different models were tested for each data set, resulting in a reduction of Chi-squared values that reach a minimum when using three discrete exponential decays. Models that included Lorentz distributions were also tested and resulted in almost equally reduced Chi-squared values while requiring fewer fitting parameters. Analysis of the 2AP residue incorporated at position 13 of the ODN (13AP) results in multiple lifetimes best represented by three exponential decays with lifetime estimates of 0.354, 3.1, and 9.07 ns, and fractional intensities of 0.166, 0.345 and 0.489, respectively. The same substitution at the 13 position was previously reported as a single exponential decay of 0.34 ns (39,40). Although our results are similar for the fastest lifetime component, the rigorous analysis done in this work elucidates a more complex 2AP lifetime profile similar to the reports of multiple fluorescence decays of 2AP upon incorporation into a nucleic acid polymer (9).

Simplifying time-resolved data analysis using Phasor diagrams

Phasor diagrams offer a model free evaluation of time-resolved results by transforming the data into phasor plot coordinates. The phase and modulation results for free 2AP and 13AP in the presence of 25 mM KCl are transformed into phasor points over the entire range of collected modulation frequencies using Equations 1 and 2 (Figure 2C). This highlights the dependence of phasor points on the chosen frequency. The phasor points are shown to have arching trajectories dependent on the fixed frequency when it is changed from 10 to 150 MHz. The free 2AP phasor points follow the arching ‘universal circle’ indicating that a single lifetime is present, whereas 13AP phasor points fall within the ‘universal circle’ due to the complex distribution of lifetimes. Figure 2D illustrates the meaning of the complex 13AP phasor points more exactly. Three lifetimes were resolved by non-linear regression for the 13AP substitution (Supplementary Table S1). These three lifetimes are indicated as phasor points on the universal circle in Figure 2D. The phasor point for the

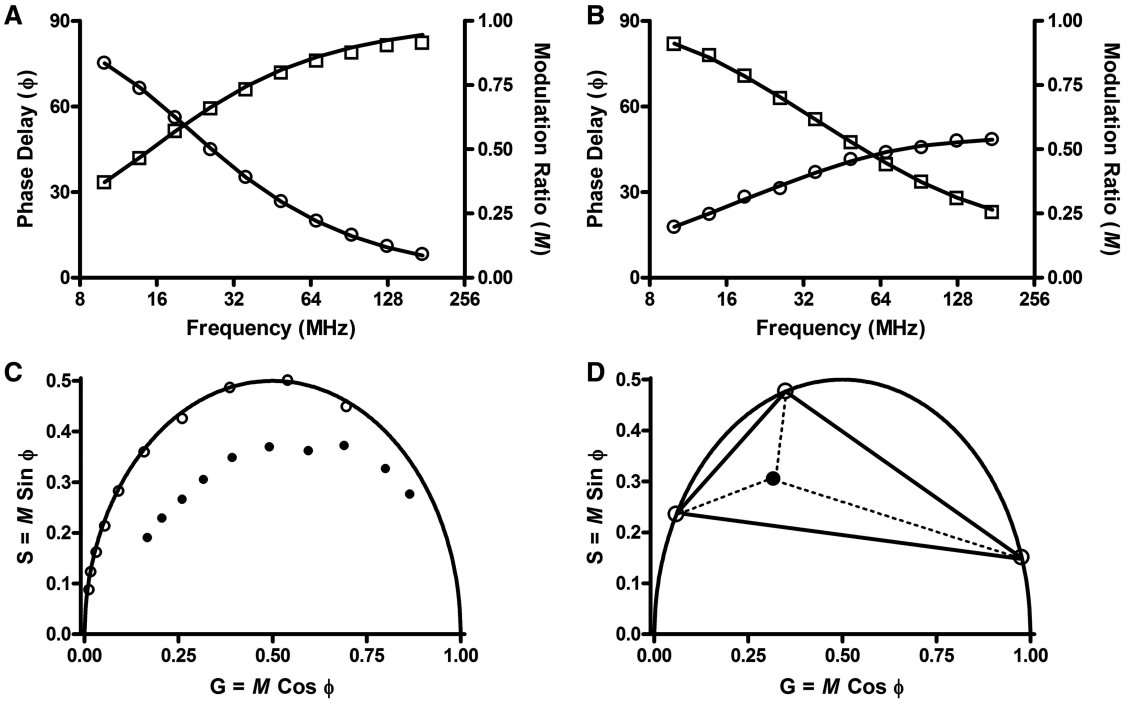

Figure 2. Phase (φ, open circles) and modulation (*M*, open squares) multi-frequency lifetime plots for free 2AP and 13AP in the presence of 25 mM KCl showing best fit lines determined from curve fitting analysis using Global software. (**A**) 2AP free in solution shows a single exponential decay with a lifetime of 10.4 ns. (**B**) The substituted 2AP deoxyoligonucleotide, 13AP, is best represented with three exponential decays with lifetimes of 0.354, 3.1, and 9.07 ns and corresponding fractional intensities of 0.166, 0.345, and 0.489, respectively. (**C**) These phase and modulation plots can be rapidly converted to phasor plots representations and analysis without the requirement of curve fitting to models. The frequency dependence is highlighted by conversion of all collected frequency data to unique phasor points for free 2AP (open circles) and 13AP (closed circles). Free 2AP demonstrates that single lifetime fluorophores will follow the arch of the universal circle when plotted against frequency. Complex decays, such as that from 13AP, exhibit similar arching behavior when plotted against frequency while remaining within the universal circle. (**D**) The phasor point for 13AP at 70 MHz (filled circle) falls within the universal circle and represents a complex mixture of fluorescent decays. Through use of the three exponential decays found from non-linear regression analysis (fractional intensity and lifetime values given above), the phasor point construction is illustrated as the mixture of the three single exponential decays (open circles).

13AP complex lifetime mixture lies within line segments connecting the three unique single exponential lifetimes. Line segments connecting the phasor points of each single lifetime and phasor point are shown in Figure 2D. These indicate that the phasor is not equidistant from each phasor point, reflecting the relative fractional intensity of each lifetime component. The exact location of the phasor point thus arises from the underlying distribution of fluorescence lifetimes and fractional intensities, and provides a unique snapshot of that complexity. Factors that influence either the underlying lifetimes or fractional intensities would result in a change in the position of the phasor point.

Phasor points were constructed for all four 2AP-labeled ODNs in the presence of 25 mM potassium or 50 mM sodium (Figure 3A). The four 2AP-substituted ODNs are described by points on the phasor plot corresponding to unique environments around each of the substitutions. All four 2AP-labeled ODN phasor points fall within the universal circle indicating a mixture of fluorescent lifetime decays. The phasor points are constructed through model free analysis, requiring no prior knowledge of the lifetime mixture or non-linear regression analysis. The significant advantage of these phasor plots is that they show, at a glance, a specific signature of particular G-quadruplex conformations. The signature for the Na^+ 'basket' form is clearly distinctive from that of the K^+ 'hybrid' form.

The errors associated with the phasor points of the four different 2AP-labeled ODNs in the presence of either KCl or NaCl were generated using Equations 3 and 4 and are shown in Figure 3B. Although the phasor points in Figure 3A show overlapping regions, this is only because the size of the points used to represent the phasors is larger than the error of the phase and modulation measurements. The enlarged phasor diagrams show that the points are well resolved on the phasor plot. Each of the 2AP-substitutions occupies a unique location on the phasor diagram reflecting the fluorophore's sensitivity to distinct G-quadruplex loop environments. A comparison between the 2AP-labeled ODNs sorted by position further demonstrates that the environment of each 2AP is unique in sodium or potassium solutions (Supplementary Figure S2). The four 2AP-labeled ODN samples result in unique phasor points between folded and unfolded conditions, as well as differences between sodium and potassium conformations. These distinct phasor points established analysis of 2AP-labeled G-quadruplexes by phasor diagrams can be used to follow changes in solution conformation.

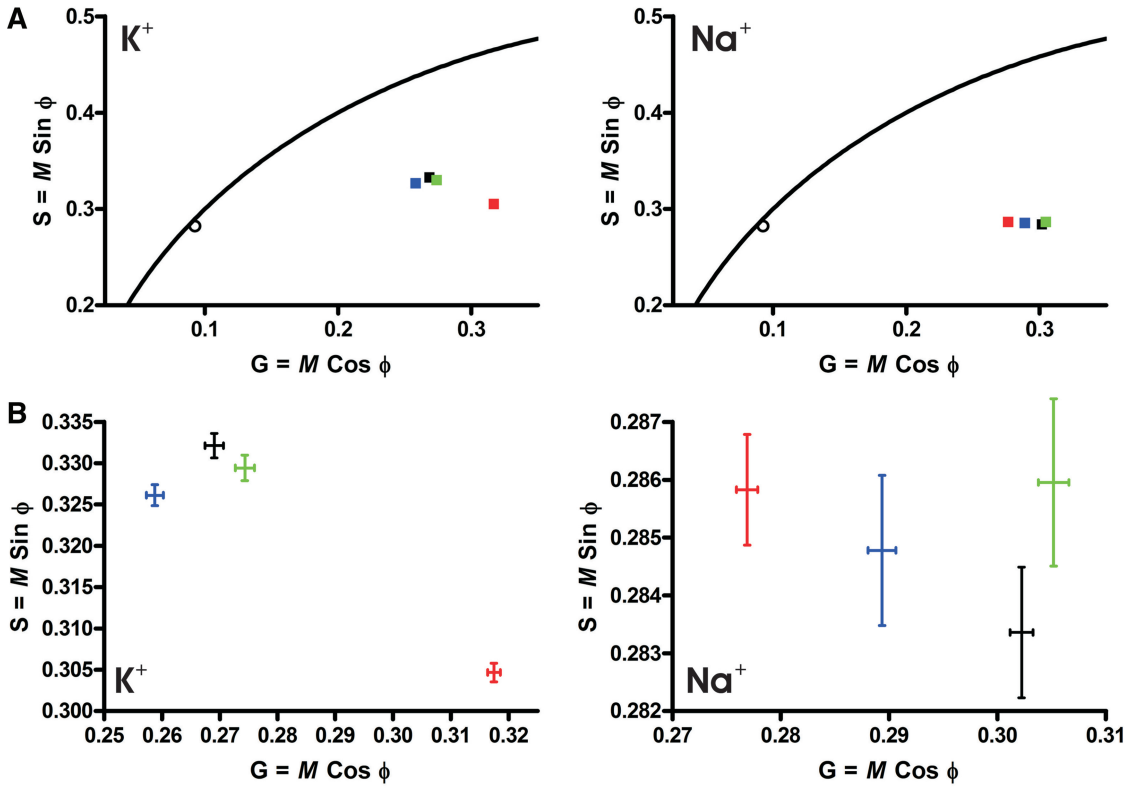

Figure 3. (**A**) Phasor diagram representations at 70 MHz of the four different 2AP-labeled deoxyoligonucleotides in the presence of either potassium or sodium with colors corresponding to Diagram 1. The 'universal circle' is represented by a solid arching line whereas the open circle phasor point demonstrates the placement of the single exponential decay from free 2AP. (**B**) The evaluation of errors associated with the phasor points for both potassium and sodium highlights differences in phasor point locations dependent on the G-Quadruplex loop in which the 2AP is placed. Any difference in the phasor point reflects a 2AP environment distinct from the placement at other positions. Both potassium and sodium phasor representations show differences between the environment of all four positions used to probe the G-quadruplex conformation.

Monitoring G-quadruplex formation through phasor diagrams

The formation of G-quadruplex structure was monitored by addition of sodium or potassium to a solution of the human telomeric G-quadruplex forming ODN. These types of experiments have determined optimal cation concentrations for G-quadruplex formation, the kinetics of G-quadruplex structural formation, and the mechanism for G-quadruplex folding (41,50,51). Figure 4A illustrates a potassium titration of 0–100 mM KCl of the 22-base telomeric G-quadruplex sequence following changes in the circular dichroism signal at 295 nm. The titration shows that the transition from an unfolded state to a folded state is complete by 5 mM KCl (41). CD is sensitive primarily to stacking of the G-quartet core and reflects global folding. Other probes, like 2AP fluorescence, provide additional information about local folding of other regions of the structure for a more complete description of the process.

The formation of the telomeric G-quadruplex structure of the 1AP and 13AP-substituted sequence was monitored by phasor representations at 93 MHz upon the addition of potassium over the range of 0–100 mM (Figure 4B). The phasor plots show multiphasic trajectories for both ODNs, with the first change occurring with large movements of the phasor point from 0 to 5 mM KCl, and a second lesser motion of the phasor point between 5 and 100 mM KCl. These phasor plots reveal subtleties in the folding process that are not evident in the titration monitored by CD. The initial phasor transition is the formation of G-quadruplex structure organized by the addition of potassium cations and stabilization of the G-tetrad core. This result parallels the data collected from circular dichroism measurements (41). The binding of potassium ions was recently shown to be the largest driving force for telomeric G-quadruplex formation (52). The time-resolved results appear to be sensitive to a second transition occurring at >5 mM KCl that was difficult to establish through CD measurements. The sensitivity of the phasor diagrams also shows differences between the two environments being probed by 1AP and 13AP substitutions. The 1AP potassium titration shows a sharp transition over the 5- to 100-mM KCl range, whereas the 13AP titration expands across a larger range of the phasor diagram. This indicates the two locations being probed are affected in different ways by the addition of potassium >5 mM. The phasor representation of the 13AP-labeled ODN is illustrated in a 3D plot to clearly show the trajectory of the phasor points against increasing concentration of KCl (Figure 4C).

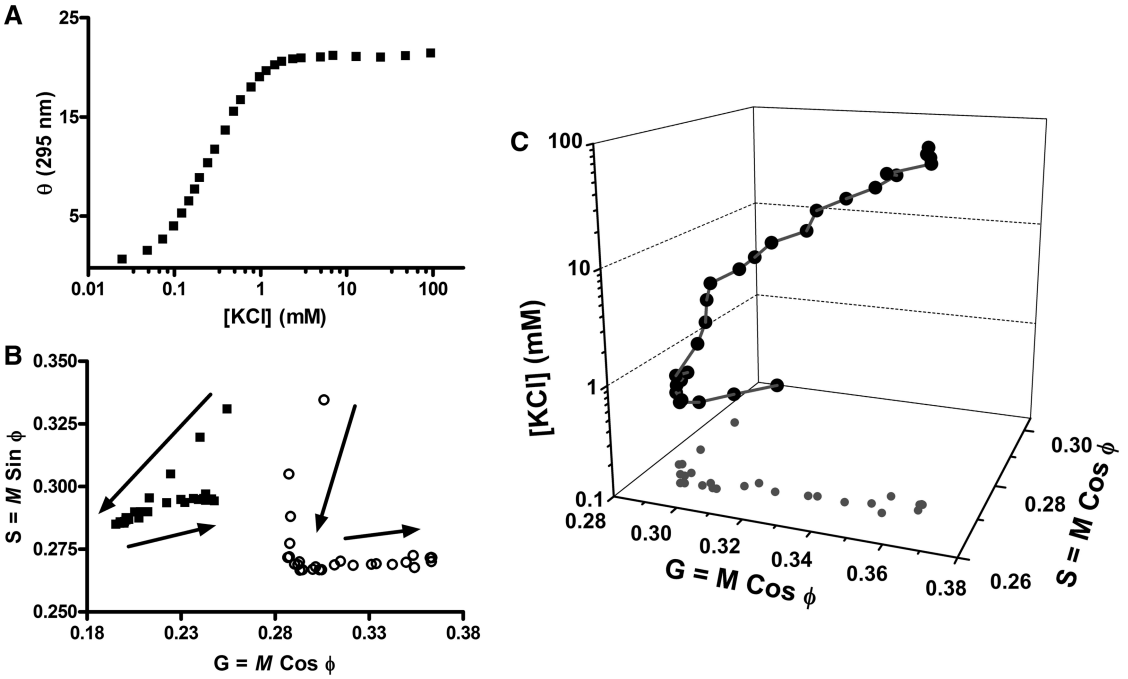

Figure 4. Monitoring changes to the 22-base G-quadruplex forming sequence upon the addition of potassium using circular dichroism and phasor plots. (**A**) Circular dichroism in millidegrees monitored at 295 nm increased dramatically upon the addition of potassium between 0.1 and 1 mM. (**B**) Phasor representations at 93 MHz monitoring changes to the fluorophore environment for 1AP (filled squares) and 13AP (open circles) G-quadruplex forming sequences. Arrows are used to trace the direction of increasing potassium concentrations. Both substitutions show a sharp and fast phasor change between 0 and 5 mM potassium, with a slow change occurring from 5 to 100 mM. The non-overlapping phasors for 1AP and 13AP correlate to differences in the environment of the 2AP, but show similar trends upon the addition of potassium. (**C**) Three-dimensional phasor representations of 13AP at 93 MHz demonstrating the phasor points change direction >1 mM potassium. Phasor representations are able to capture small changes during the folding of G-quadruplex DNA upon the addition of cation and can be used to locally monitor specific loop regions.

Digestion of G-quadruplex structure through Mung Bean Nuclease digestions

The single-strand specific mung bean nuclease offers an alternative method to probing the accessibility of G-quadruplex loop regions. Mung bean nuclease has been used to selectively digest loops in the study of DNA hairpin conformations (53,54), suggesting it may also be a useful probe for intramolecular G-quadruplex loops. The endonucleolytic activity of mung bean nuclease has also been found to preferentially digest around adenosine residues (55). Therefore, digestion of telomeric G-quadruplex structures should occur preferentially at the –TTA– loops. Evaluation of digestion kinetics for known G-quadruplex loops (double-chain reversal, edgewise, diagonal) may allow for conclusions to be drawn on the type of loops present in unknown G-quadruplex structures. Digestion kinetics can be used in conjunction with similar techniques such as fluorescence quenching, allowing for an accessibility profile of loop geometries to be established.

The digestion profiles of mung bean nuclease with the 13AP-labeled telomeric G-quadruplex forming sequence in the presence of potassium were evaluated using both steady-state and time-resolved fluorescence techniques. Steady-state digestion profiles of the 13AP-labeled telomeric G-quadruplex structure show a complex time course with a leading lag phase lasting ~3000 s (Figure 5A). Following the initial digestion lag phase, a sharp rise in the total fluorescent intensity occurs between 3000 and 15 000 s, where the emission intensity reaches a plateau of 10 times the initial intensity.

The time-resolved phasor diagram shows two unique phasor trajectories during the digestion time course (Figure 5B). The initial phasor trajectory corresponds with the steady-state lag phase and is proposed to be an initial slow digestion of the telomeric G-quadruplex loops. The second phasor trajectory, which expands downward toward the universal circle, corresponds to the large increase in the emission intensity seen from steady-state digestions. This portion of the digestion profile is proposed to be the digestion of single-stranded DNA after destabilization of the G-quadruplex structure has occurred, resulting from one or more nucleolytic nicks.

At digestion completion the phasor points remain stationary at approximately $G,S = (0.11, 0.23)$, a phasor coordinate located inside of the universal circle. Although mung bean nuclease has been shown to digest DNA to the single nucleotide level (55), the phasor diagram suggests that mung bean nuclease may not completely excise the 2AP from the nucleic acid polymer. If 2AP was completely excised from the nucleic acid polymer, this would result in a phasor point corresponding to a single lifetime similar to that of free 2AP measurements. Another possible explanation for failure of the phasor point to reach the universal circle after prolonged digestion is that the lifetime of 2AP may be influenced by the

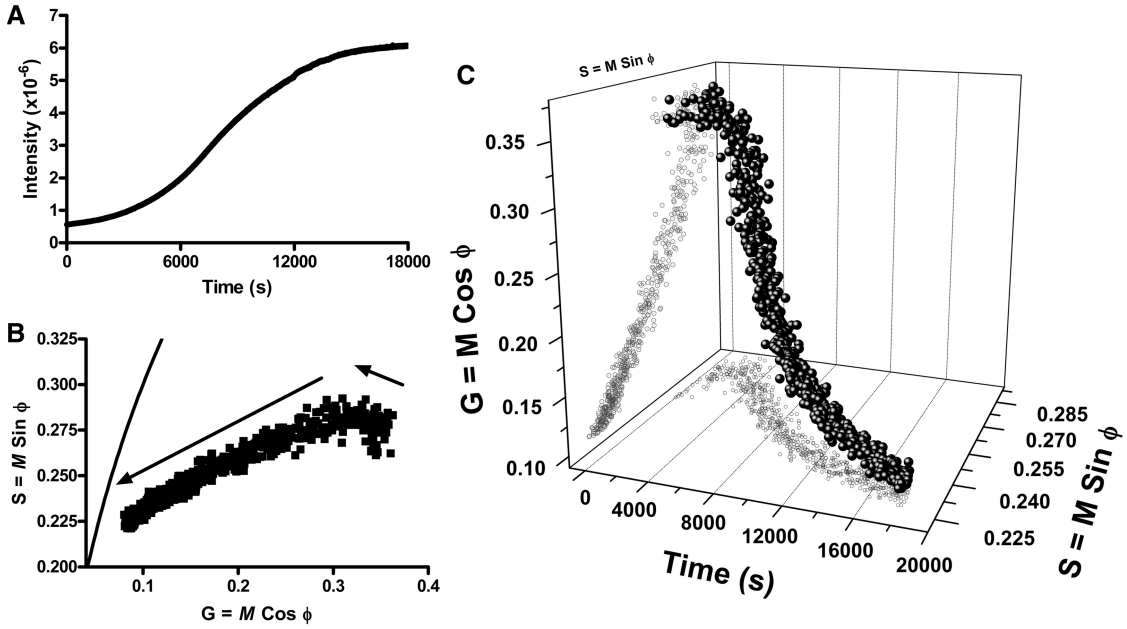

Figure 5. (**A**) Steady-state fluorescence monitoring of the mung bean nuclease digestions of 13AP shows an initial lag phase of ~3000 s following by an exponential digestion state before leveling off after 15 000 s. (**B**) Phasor representation at 93 MHz of the mung bean nuclease digestion of 13AP demonstrates two unique phasor changes. Arrows indicate the direction of increasing time. The universal circle is drawn as a solid arching line. The initial change of the phasor is upward and continues for 3000–4000 s. The second phasor change continued until 16 000 s at which point the phasor point remained nearly constant at *G*,*S* coordinates (0.11, 0.23). (**C**) Representation of the phasor diagram in a 3D plot emphasizing the change in (*G*,*S*) against time.

presence 5′-phosphate and 3′-hydroxyl groups. The impacts of these linkages on 2AP lifetime have not been established.

To emphasize the time course of the digestion profile, the *G* and *S* coordinates are plotted against time in 3D space (Figure 5C). When plotted against time, the phasor diagram shows the same digestion curve as the steady-state results, establishing the phasor diagram inherently contains the same information as the steady-state curve while allowing for more detailed conclusions to be drawn. These fluorescence based digestions show that phasors are able to monitor the degradation of G-quadruplexes and result in sensitive digestion profiles. For the scope of this manuscript, precise kinetic models were not evaluated using the resulting steady-state or time-resolved digestion profiles. Detailed kinetic analysis of G-quadruplex loops by mung bean nuclease will be investigated in future work with the potential for establishing accessibility profiles for known loop geometries.

Phasor interpretation of quencher accessibility

Another important fluorescence technique in the study of G-quadruplex structure is collisional quenching (7). The accessibility of singly substituted 2AP residues to quenching by acrylamide has been used to probe the loops of human telomeric G-quadruplexes (43). Stern–Volmer plots constructed for acrylamide quenching of the 13AP telomeric G-quadruplex show characteristic downward curvature, distinct from the quenching of high accessible 2AP free in solution (Figure 6A). Downward curvature of the Stern–Volmer quenching plots indicates heterogeneity in the 2AP environment, which can result from either multiple global G-quadruplex conformations or distinct localized position of the fluorophore within the G-quadruplex loop. The downward curvature of these Stern–Volmer plots is distinct from the quenching of 2AP nucleotides free in solution, which demonstrate a linear dependence to added quencher and were determined to have a diffusion limited quenching constant (Figure 6B).

A method for partitioning the number of components necessary for analyzing the downward curvature is to identify by time-resolved techniques multiple lifetime components (56). Time-resolved fluorescence techniques offer sensitive measurements of multiple 2AP environments based on lifetimes, which can then be used to construct individual lifetime Stern–Volmer (τ_0/τ against quencher concentration) plots. The lifetime-based τ_0/τ plots can be used to establish Stern–Volmer quenching constants for individual components and relate directly to the type of quenching process (56). The addition of acrylamide to the 13AP telomeric G-quadruplex sequence was used to construct an average τ_0/τ quenching plot for the time-resolved measurements and compared with steady-state intensity measurements (Figure 6A). The average lifetime plot shows the same downward curvature present from the steady-state plot, indicating the multiple fraction model accurately represents steady-state experiments. The differences between the two curves are due to the inability to accurately fit the mixture of lifetimes present, made difficult by the large number of components present with a wide range of lifetimes (10 ns to <1 ns lifetimes) along

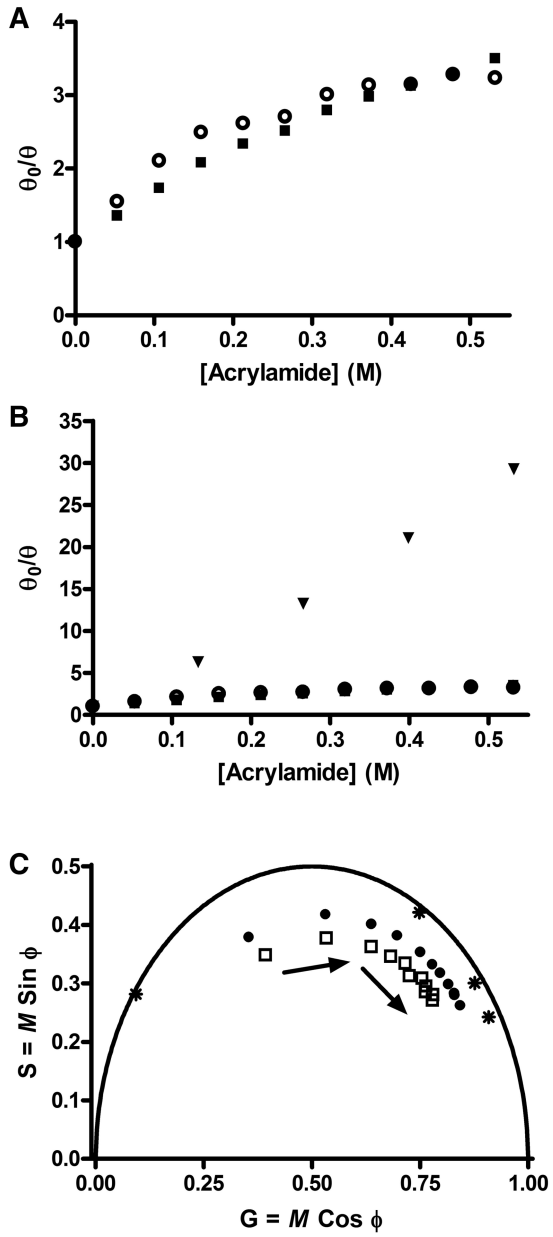

Figure 6. (**A**) Stern–Volmer quenching plots constructed from fluorescent intensity (F_0/F—filled squares) and average lifetime (τ_0/τ—open circles) for the addition of acrylamide to 13AP. The Stern–Volmer plots show downward curvature for both intensity and average lifetime indicating multiple accessible 2AP populations. (**B**) Stern–Volmer plots comparing acrylamide quenching of free 2AP (triangles) with the fluorescent intensity and averaged lifetime of 13AP. The quenching of free 2AP shows diffusion limited accessibility to quenching by acrylamide. (**C**) Quenching of 1AP (filled circles) and 13AP (open boxes) by acrylamide monitored using phasors at 49 MHz. Arrows indicate the direction of increasing acrylamide concentration. Phasor diagram shows an initial fast change in phasor position followed by a slower moving phasor change. The quenching of free 2AP (stars) by acrylamide analyzed by phasor diagrams is located initially on the universal circle with slow deviation from the universal circle at high acrylamide concentrations. This is proposed to be a similar deviation from a single lifetime component as was previously reported in glycerol/water mixtures (10), or small background interference being seen at high quencher concentrations.

with the addition of quencher to this complex mixture. The ability to dissect the mixture of lifetimes into discrete components through model dependent methods becomes increasingly difficult with the addition of quencher. Because the lifetime mixture of 13AP contains very fast fluorescent decays (<1 ns), and the addition of quencher causes this species to act as though the lifetime has decreased, the sensitivity to analyze lifetime components this short decreases significantly.

Phasors monitor the quenching of the complex 2AP lifetime mixture without detailed analysis by model dependent methods. Acrylamide quenching of 1AP and 13AP telomeric G-quadruplex sequences in the presence of potassium presents arching phasor trajectories with increasing acrylamide concentration (Figure 6C). The arching phasor trajectories collected at a fixed modulation frequency signify decreasing lifetimes in solution (19). The phasor points do not converge to the universal circle, implying the phasor method is sensitive to the multiple lifetimes present in solution, even at high acrylamide concentrations. The arching phasor trajectory is equivalent to that seen for the quenching of free 2AP in solution. Interestingly, the free 2AP acrylamide quenching trajectories show a gradual deviation from the universal circle at high acrylamide concentrations. This matches previous reports that the lifetime of 2AP increases in complexity from a single exponential decay upon quenching with acrylamide (10). However, this earlier report used glycerol/water mixtures of 2AP and hence cannot be directly compared with our results. It is also possible that a small unquenched background fluorescence could explain the deviation of the phasor point from the universal circle at high acrylamide levels. Phasor diagrams result in the ability to track shortening lifetime mixtures that would otherwise be difficult to analyze by normal non-linear regression methods.

Evaluation of FRET by phasors

FRET has become an important aspect of G-quadruplex solution studies because of the ability to determine molecular distance and interaction. FRET-labeled G-quadruplex forming sequences have served to elucidate folding pathways and kinetics, while single-molecule FRET studies have investigated G-quadruplex solution heterogeneity (44,45). FRET-labeled G-quadruplex structures can also be used in thermal denaturation studies to determine the stability of the conformation, and can serve for high-throughput analysis using fluorescence detecting thermal cyclers (46,47). Although many of these techniques rely on the fluorescence emission of either the acceptor or donor fluorophore to monitor change, the use of FRET in time-resolved instrumentation is directly related to lifetime, as the decrease in lifetime equates directly to the efficiency of energy transfer (57).

Potassium and sodium titrations were completed using a FAM/TAMRA dual-labeled 22-nt human telomeric G-quadruplex forming sequence where both the emission intensity and frequency-domain lifetime measurements were collected (Figure 7). Filter sets were used for the collection of fluorescence emission of only FAM. Total

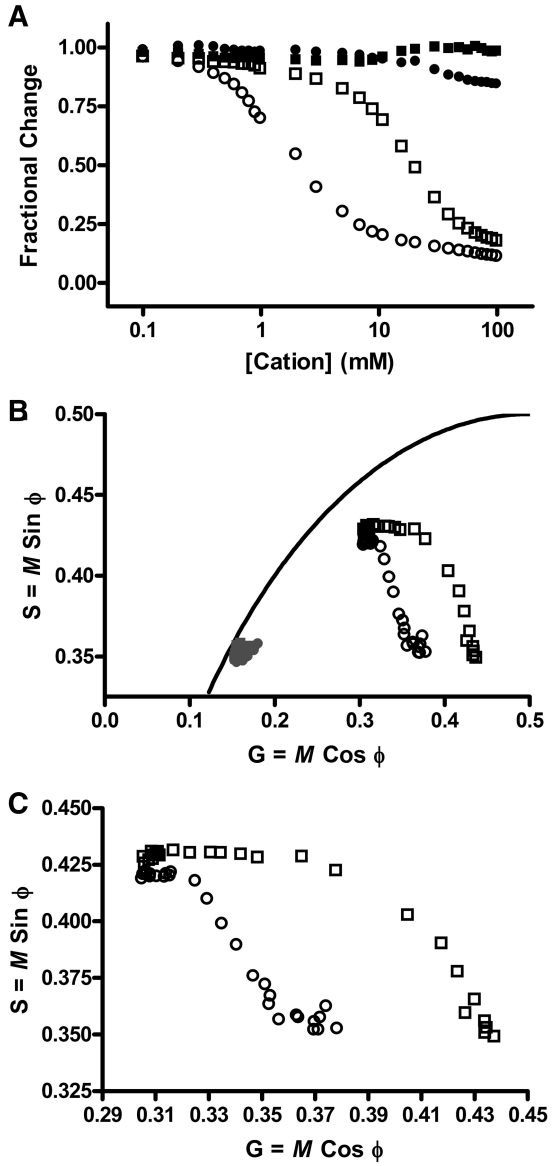

Figure 7. G-quadruplex folding monitored through changes in FRET efficiencies using donor alone (FAM) and donor-acceptor (FAM-TAMRA) labeled human telomeric 22-base sequences upon the addition of potassium (circles) or sodium (boxes). (**A**) G-quadruplex folding was monitored by total fluorescence intensity upon the addition of cation over a range of 0–100 mM. Both potassium and sodium show a single significant transition with midpoints at 5 and 25 mM, respectively. The background intensities from potassium (filled circles) and sodium (filled boxes) titrations using donor alone show minimal changes in total intensity. (**B**) Phasor diagrams using 93 MHz frequency were prepared from the same titrations used for total intensity. Solid arching line represents the universal circle. The donor alone samples (closed circles and squares) show no movement and remain near the universal circle with increasing cation concentration, whereas dual-labeled telomeric 22-base DNA shows phasor points distinct from donor alone and significant trajectories with increasing cation concentration. (**C**) Enlarged phasor diagrams emphasizing motion of the phasor point with cation titrations. Potassium phasors (circles) show two unique trajectories with movement downward over the potassium range 3–30 mM and movement right from 30 to 100 mM. Sodium (squares) shows only a single trajectory with significant movement over the range 15–100 mM.

intensity measurements using the FAM/TAMRA ODN show a decrease in the emission intensity of FAM upon the introduction of cation. This decrease in fluorescence emission intensity is caused by the formation of G-quadruplex, bringing the FAM/TAMRA pair closer together and allowing for increased efficiency of energy transfer. This change is distinct from titrations conducted using donor-alone ODN. When the 22-nt ODN is labeled with only FAM, the change in total intensity is <10% (Figure 7A). This small change with the FAM-only ODN indicates the change seen from the FAM/TAMRA dual-labeled ODN corresponds to energy transfer and not an influence on the fluorescence intensity due to the addition of cation. The potassium titration has a midpoint of 5 mM, similar to that found from the 2AP titrations, whereas the sodium titration has a significantly higher midpoint at 25 mM. These results match previous telomeric G-quadruplex folding studies (41).

The FRET phasor diagrams track global conformational changes through the folding of the G-quadruplex upon the addition of cation. The FAM-only 22-nt ODN sodium or potassium titration phasor diagrams overlay near the universal circle and show no movement with increasing concentration of cation (Figure 7B). This demonstrates the phasor diagrams are not sensitive to the changes in G-quadruplex folding without the presence of the acceptor. The FAM/TAMRA dual-labeled sodium titration phasor diagram shows a single trajectory across the sodium concentration range. The phasor points move from an initial position of (0.31, 0.425) to a final position of (0.43, 0.35) (Figure 7C). The phasor trajectory indicates only a single conformation change over the sodium concentration range of 0–100 mM. Interestingly, the potassium titration of the FAM/TAMRA dual-labeled ODN shows two trajectories similar to that obtained from 2AP-labeled samples. An initial phasor trajectory is present upon the addition of potassium from 3 to 30 mM, with significant downward movement of the phasor points. The phasor points then shift outward during the range of 30–100 mM potassium, indicating sensitivity to a secondary global conformational change from the time-resolved measurements. The phasor points should remain stationary unless there is continued influence on the fluorophore's environment, similar to the phasor diagram shown for sodium titrations. This secondary transition was present in both the 2AP-labeled titrations and FRET-labeled titrations, and seen only through the use of time-resolved methodologies.

SUMMARY

Phasor diagrams provided a simplified but highly informative representation of time-resolved fluorescence data. We show the utility of phasors for analysis of strategically substituted 2AP or FRET-labeled G-quadruplex studies. Phasor plot trajectories using these probes reveal subtle aspects of G-quadruplex conformational transitions that are often not evident in steady-state fluorescence, circular dichroism or absorbance measurements, thus providing novel insights into the underlying reaction mechanisms.

We show the utility of phasor diagrams for providing signatures of different human telomere G-quadruplex conformations, monitoring cation-driven folding, evaluating nuclease digestion reactions and visualizing complex collisional quenching reactions. As is the case for most electronic spectroscopies (absorbance, CD, steady-state fluorescence), phasor diagrams cannot provide high-resolution structural details about G-quadruplexes, but are of significant value in monitoring changes in conformation driven by changes in solution conditions. Phasor diagrams have seen little, if any, use in time-resolved fluorescence studies of nucleic acids. We show here their value for revealing new information about G-quadruplex transitions not available by other spectroscopic tools.

SUPPLEMENTARY DATA

Supplementary Data are available at NAR Online: Supplementary Table S1 and Supplementary Figures S1 and S2.

ACKNOWLEDGEMENTS

The authors wish to thank Dr Justin Ross for his assistance with some preliminary lifetime measurements and Dr Robert D. Gray for many helpful discussions.

FUNDING

Research funded by grant CA35635 from the National Cancer Institute of the National Institutes of Health and by the James Graham Brown Foundation. Funding for open access charge: National Cancer Institute (CA35635); James Graham Brown Foundation.

Conflict of interest statement. None declared.

REFERENCES

1. Ward,D.C., Reich,E. and Stryer,L. (1969) Fluorescence studies of nucleotides and polynucleotides. I. Formycin, 2-aminopurine riboside, 2,6-diaminopurine riboside, and their derivatives. *J. Biol. Chem.*, **244**, 1228–1237.
2. Reha-Krantz,L.J. (2009) The use of 2-aminopurine fluorescence to study DNA polymerase function. *Methods Mol. Biol.*, **521**, 381–396.
3. Tang,G.Q., Anand,V.S. and Patel,S.S. (2011) Fluorescence-based assay to measure the real-time kinetics of nucleotide incorporation during transcription elongation. *J. Mol. Biol.*, **405**, 666–678.
4. Sarkar,K., Nguyen,D.A. and Gruebele,M. (2010) Loop and stem dynamics during RNA hairpin folding and unfolding. *RNA*, **16**, 2427–2434.
5. Sarkar,K., Meister,K., Sethi,A. and Gruebele,M. (2009) Fast folding of an RNA tetraloop on a rugged energy landscape detected by a stacking-sensitive probe. *Biophys. J.*, **97**, 1418–1427.
6. Degtyareva,N.N. and Petty,J.T. (2011) Non-B conformations of CAG repeats using 2-aminopurine. *Methods Enzymol.*, **492**, 213–231.
7. Gray,R.D., Petraccone,L., Buscaglia,R. and Chaires,J.B. (2010) 2-aminopurine as a probe for quadruplex loop structures. *Methods Mol. Biol.*, **608**, 121–136.
8. Ballin,J.D., Prevas,J.P., Bharill,S., Gryczynski,I., Gryczynski,Z. and Wilson,G.M. (2008) Local RNA conformational dynamics revealed by 2-aminopurine solvent accessibility. *Biochemistry*, **47**, 7043–7052.
9. Guest,C.R., Hochstrasser,R.A., Sowers,L.C. and Millar,D.P. (1991) Dynamics of mismatched base pairs in DNA. *Biochemistry*, **30**, 3271–3279.
10. Bharill,S., Sarkar,P., Ballin,J.D., Gryczynski,I., Wilson,G.M. and Gryczynski,Z. (2008) Fluorescence intensity decays of 2-aminopurine solutions: lifetime distribution approach. *Anal. Biochem.*, **377**, 141–149.
11. Fogarty,A.C., Jones,A.C. and Camp,P.J. (2011) Extraction of lifetime distributions from fluorescence decays with application to DNA-base analogues. *Phys. Chem. Chem. Phys.*, **13**, 3819–3830.
12. Rachofsky,E.L., Osman,R. and Ross,J.B. (2001) Probing structure and dynamics of DNA with 2-aminopurine: effects of local environment on fluorescence. *Biochemistry*, **40**, 946–956.
13. Jean,J.M. and Hall,K.B. (2001) 2-Aminopurine fluorescence quenching and lifetimes: role of base stacking. *Proc. Natl Acad. Sci. USA*, **98**, 37–41.
14. Jean,J.M. and Hall,K.B. (2002) 2-Aminopurine electronic structure and fluorescence properties in DNA. *Biochemistry*, **41**, 13152–13161.
15. Brochon,J.C. (1994) Maximum-entropy method of data-analysis in time-resolved spectroscopy. *Method Enzymol.*, **240**, 262–311.
16. Stefl,M., James,N.G., Ross,J.A. and Jameson,D.M. (2011) Applications of phasors to in vitro time-resolved fluorescence measurements. *Anal. Biochem.*, **410**, 62–69.
17. Cole,K.S. and Cole,R.H. (1941) Dispersion and absorption in dielectrics I. Alternating current characteristics. *J. Chem. Phys.*, **9**, 341–351.
18. Clayton,A.H., Hanley,Q.S. and Verveer,P.J. (2004) Graphical representation and multicomponent analysis of single-frequency fluorescence lifetime imaging microscopy data. *J. Microsc.*, **213**, 1–5.
19. Redford,G.I. and Clegg,R.M. (2005) Polar plot representation for frequency-domain analysis of fluorescence lifetimes. *J. Fluoresc.*, **15**, 805–815.
20. Jameson,D.M., Gratton,E. and Hall,R.D. (1984) The measurement and analysis of heterogeneous emissions by multifrequency phase and modulation fluorometry. *App. Spectroscopy Rev.*, **20**, 55–106.
21. Weber,G. (1981) Resolution of the fluorescence lifetimes in a heterogeneous system by phase and modulation measurements. *J. Phys. Chem.*, **85**, 949–953.
22. Hanley,Q.S. (2009) Spectrally resolved fluorescent lifetime imaging. *J. R. Soc. Interface*, **6**, S83–S92.
23. Digman,M.A., Caiolfa,V.R., Zamai,M. and Gratton,E. (2008) The phasor approach to fluorescence lifetime imaging analysis. *Biophys. J.*, **94**, L14–L16.
24. Wouters,F.S. and Esposito,A. (2008) Quantitative analysis of fluorescence lifetime imaging made easy. *HFSP J.*, **2**, 7–11.
25. Leray,A., Spriet,C., Trinel,D., Blossey,R., Usson,Y. and Heliot,L. (2011) Quantitative comparison of polar approach versus fitting method in time domain FLIM image analysis. *Cytometry A*, **79**, 149–158.
26. James,N.G., Ross,J.A., Stefl,M. and Jameson,D.M. (2011) Applications of phasor plots to in vitro protein studies. *Anal. Biochem.*, **410**, 70–76.
27. Lane,A.N., Chaires,J.B., Gray,R.D. and Trent,J.O. (2008) Stability and kinetics of G-quadruplex structures. *Nucleic Acids Res.*, **36**, 5482–5515.
28. Huppert,J.L. (2008) Four-stranded nucleic acids: structure, function and targeting of G-quadruplexes. *Chem. Soc. Rev.*, **37**, 1375–1384.
29. Yang,D. and Okamoto,K. (2010) Structural insights into G-quadruplexes: towards new anticancer drugs. *Future Med. Chem.*, **2**, 619–646.
30. Parkinson,G.N., Lee,M.P. and Neidle,S. (2002) Crystal structure of parallel quadruplexes from human telomeric DNA. *Nature*, **417**, 876–880.
31. Lim,K.W., Amrane,S., Bouaziz,S., Xu,W., Mu,Y., Patel,D.J., Luu,K.N. and Phan,A.T. (2009) Structure of the human telomere in K+ solution: a stable basket-type G-quadruplex with only two G-tetrad layers. *J. Am. Chem. Soc.*, **131**, 4301–4309.

32. Zhang,Z., Dai,J., Veliath,E., Jones,R.A. and Yang,D. (2010) Structure of a two-G-tetrad intramolecular G-quadruplex formed by a variant human telomeric sequence in K+ solution: insights into the interconversion of human telomeric G-quadruplex structures. *Nucleic Acids Res.*, **38**, 1009–1021.
33. Wang,Y. and Patel,D.J. (1993) Solution structure of the human telomeric repeat d[AG3(T2AG3)3] G-tetraplex. *Structure*, **1**, 263–282.
34. Dai,J., Carver,M., Punchihewa,C., Jones,R.A. and Yang,D. (2007) Structure of the Hybrid-2 type intramolecular human telomeric G-quadruplex in K+ solution: insights into structure polymorphism of the human telomeric sequence. *Nucleic Acids Res.*, **35**, 4927–4940.
35. Dai,J., Punchihewa,C., Ambrus,A., Chen,D., Jones,R.A. and Yang,D. (2007) Structure of the intramolecular human telomeric G-quadruplex in potassium solution: a novel adenine triple formation. *Nucleic Acids Res.*, **35**, 2440–2450.
36. Phan,A.T., Luu,K.N. and Patel,D.J. (2006) Different loop arrangements of intramolecular human telomeric (3+1) G-quadruplexes in K+ solution. *Nucleic Acids Res.*, **34**, 5715–5719.
37. Luu,K.N., Phan,A.T., Kuryavyi,V., Lacroix,L. and Patel,D.J. (2006) Structure of the human telomere in K+ solution: an intramolecular (3 + 1) G-quadruplex scaffold. *J. Am. Chem. Soc.*, **128**, 9963–9970.
38. Ambrus,A., Chen,D., Dai,J., Bialis,T., Jones,R.A. and Yang,D. (2006) Human telomeric sequence forms a hybrid-type intramolecular G-quadruplex structure with mixed parallel/antiparallel strands in potassium solution. *Nucleic Acids Res.*, **34**, 2723–2735.
39. Kimura,T., Kawai,K., Fujitsuka,M. and Majima,T. (2004) Fluorescence properties of 2-aminopurine in human telomeric DNA. *Chem. Commun.*, 1438–1439.
40. Kimura,T., Kawai,K., Fujitsuka,M. and Majima,T. (2007) Monitoring G-quadruplex structures and G-quadruplex-ligand complex using 2-aminopurine modified oligonucleotides. *Tetrahedron*, **63**, 3585–3590.
41. Gray,R.D., Petraccone,L., Trent,J.O. and Chaires,J.B. (2010) Characterization of a K+-induced conformational switch in a human telomeric DNA oligonucleotide using 2-aminopurine fluorescence. *Biochemistry*, **49**, 179–194.
42. Petraccone,L., Garbett,N.C., Chaires,J.B. and Trent,J.O. (2010) An integrated molecular dynamics (MD) and experimental study of higher order human telomeric quadruplexes. *Biopolymers*, **93**, 533–548.
43. Li,J., Correia,J.J., Wang,L., Trent,J.O. and Chaires,J.B. (2005) Not so crystal clear: the structure of the human telomere G-quadruplex in solution differs from that present in a crystal. *Nucleic Acids Res.*, **33**, 4649–4659.
44. Okamoto,K., Sannohe,Y., Mashimo,T., Sugiyama,H. and Terazima,M. (2008) G-quadruplex structures of human telomere DNA examined by single molecule FRET and BrG-substitution. *Bioorg. Med. Chem.*, **16**, 6873–6879.
45. Shirude,P.S. and Balasubramanian,S. (2008) Single molecule conformational analysis of DNA G-quadruplexes. *Biochimie*, **90**, 1197–1206.
46. De Cian,A., Guittat,L., Kaiser,M., Sacca,B., Amrane,S., Bourdoncle,A., Alberti,P., Teulade-Fichou,M.P., Lacroix,L. and Mergny,J.L. (2007) Fluorescence-based melting assays for studying quadruplex ligands. *Methods*, **42**, 183–195.
47. De Cian,A., Guittat,L., Shin-ya,K., Riou,J.F. and Mergny,J.L. (2005) Affinity and selectivity of G4 ligands measured by FRET. *Nucleic Acids Symp. Ser.*, **49**, 235–236.
48. Barbieri,B., Terpetschnig,E. and Jameson,D.M. (2005) Frequency-domain fluorescence spectroscopy using 280-nm and 300-nm light-emitting diodes: measurement of proteins and protein-related fluorophores. *Anal. Biochem.*, **344**, 298–300.
49. Beechem,J.M. and Gratton,E. (1988) Flourescence spectroscopy data analysis environment a second generation global analysis program. In: Lakowicz,J. (ed.), *Time-Resolved Laser Spectroscopy in Biochemistry*, Vol. 909. SPIE, Bellingham, WA, pp. 70–81.
50. Gray,R.D. and Chaires,J.B. (2008) Kinetics and mechanism of K+- and Na+-induced folding of models of human telomeric DNA into G-quadruplex structures. *Nucleic Acids Res.*, **36**, 4191–4203.
51. Gray,R.D., Li,J. and Chaires,J.B. (2009) Energetics and kinetics of a conformational switch in G-quadruplex DNA. *J. Phys. Chem. B*, **113**, 2676–2683.
52. Gray,R.D. and Chaires,J.B. (2011) Linkage of cation binding and folding in human telomeric quadruplex DNA. *Biophys. Chem.*, **159**, 205–209.
53. Baumann,U., Frank,R. and Blocker,H. (1986) Conformational analysis of hairpin oligodeoxyribonucleotides by a single-strand-specific nuclease. *Eur. J. Biochem.*, **161**, 409–413.
54. Xodo,L.E., Manzini,G., Quadrifoglio,F., van der Marel,G. and van Boom,J. (1991) DNA hairpin loops in solution. Correlation between primary structure, thermostability and reactivity with single-strand-specific nuclease from mung bean. *Nucleic Acids Res.*, **19**, 1505–1511.
55. Sung,S.C. and Laskowski,M. Sr (1962) A nuclease from mung bean sprouts. *J. Biol. Chem.*, **237**, 506–511.
56. Laws,W.R. and Contino,P.B. (1992) Fluorescence quenching studies: analysis of nonlinear Stern-Volmer data. *Methods Enzymol.*, **210**, 448–463.
57. Klostermeier,D. and Millar,D.P. (2001) Time-resolved fluorescence resonance energy transfer: a versatile tool for the analysis of nucleic acids. *Biopolymers*, **61**, 159–179.